Editors' Suggestion

Electron-Beam Source with a Superconducting Niobium Tip

C.W. Johnson,[1] A.K. Schmid,[1] M. Mankos,[2] R. Röpke,[3] N. Kerker,[3] I.S. Hwang,[4] E.K. Wong,[1] D.F. Ogletree,[1] A.M. Minor,[1,5] and A. Stibor[1,2,3,*]

[1] *Lawrence Berkeley National Laboratory, Molecular Foundry, Berkeley, California 94720, USA*
[2] *Electron Optica Inc., Palo Alto, California 94303, USA*
[3] *Institute of Physics and LISA$^+$, University of Tübingen, 72074 Tübingen, Federal Republic of Germany*
[4] *Institute of Physics, Academia Sinica, Nankang, Taipei City 115201, Taiwan, Republic of China*
[5] *Department of Materials Science and Engineering, University of California, Berkeley, California 94720-1760, USA*

(Received 29 November 2022; accepted 6 February 2023; published 10 March 2023)

Modern electron microscopy and spectroscopy are key technologies for studying the structure and composition of quantum and biological materials in fundamental and applied sciences. High-resolution spectroscopic techniques and aberration-corrected microscopes are often limited by the relatively large energy distribution of currently available beam sources. This can be improved by a monochromator, with the significant drawback of losing most of the beam current. Here, we study the field-emission properties of a monocrystalline niobium-tip electron field emitter at 5.2 K, well below the superconducting transition temperature. The emitter fabrication process can generate two tip configurations, with or without a nanoprotrusion at the apex, strongly influencing the field-emission energy distribution. The geometry without the nanoprotrusion has nanoampere beam currents, long-term stability, and an energy width of around 100 meV. The beam current can be increased by 2 orders of magnitude by xenon-gas adsorption. We also study the emitter performance up to 82 K and demonstrate that the energy width of the beam can be below 40 meV with high emitter brightness even at liquid-nitrogen cooling temperatures when an apex nanoprotrusion is present. Furthermore, the spatial and temporal electron-electron correlations of the field emission are studied at normal and superconducting temperatures and the influence of Nottingham heating is discussed. This monochromatic source will allow exceptional accuracy and resolution in electron microscopy, spectroscopy, and high-coherence quantum applications.

DOI: 10.1103/PhysRevApplied.19.034036

I. INTRODUCTION

Electron-beam field emitters are foundational in modern electron-optical applications. The performance of electron microscopes [1,2], interferometers [3–5], sensors [6], and quantum information-science applications [7] relies on intense, stable, coherent, and monochromatic beam sources with high brightness. The development of unique beam sources exploiting their nanoscopic quantum environment is opening up several areas in microscopy, such as laser-pulsed tip emitters [8,9] allowing pulse-probe microscopy of dynamic behavior on the nanosecond scale, single-atom tips [10–12] for matter-wave experiments with high coherence, or carbon-nanotube field emitters [13] with high brightness. Recently, a microengineered LaB_6 nanowire-based electron source with an on-tip integrated passive collimator has achieved atomic resolution in a transmission electron microscope [14] and a highly monochromatic cold flat single-crystal Cu(100) surface source based on near-threshold photoemission has been reported [15]. However, commercialized-microscope hot Schottky field emitters typically have energy widths of $\Delta E \approx 750$ meV and "cold" (meaning room-temperature) field emitters have $\Delta E \approx 300$ meV. This large energy distribution limits current state-of-the-art analytical methods in electron microscopy, such as high-resolution vibrational spectroscopy [16] or surface-sensitive imaging techniques such as low-energy electron microscopy (LEEM) [17]. The energy distribution can be reduced down to 9 meV [16] by the application of monochromators [18] but this removes most of the beam current and results in significantly extended measurement times, potentially causing problems with sample stability. There is a need for stable, bright, and coherent electron emitters with intrinsically narrow energy distributions.

Such a source is described in this paper. We demonstrate the fabrication of a monocrystalline niobium- (Nb) tip electron field emitter and analyze the emission properties at a superconducting temperature of 5.2 K. The emitter has

*astibor@lbl.gov

extremely low energy spreads, high beam currents, and different modes of operation that depend on the apex surface geometry of the tip. This paper complements our recent work in Ref. [19], where we have demonstrated that a nanoprotrusion (NP) can be formed on top of such a Nb tip by a specific annealing procedure, causing a distinct self-focusing field geometry. We further label such an emitter as a nanoprotrusion tip (NPT). The space confinement in the NP leads to localized quantum band states at the apex [19–24]. The field-emission energy spectra are Lorentzian shaped and can be shifted in energy relative to the sharp, low-temperature Fermi edge, cutting off the energy distribution for even smaller energy widths. This leads to energy distributions down to 16 meV full width at half maximum (FWHM), an emission angle of 3.2°, and a highly reduced brightness of up to 5.0×10^8 A/(m^2 sr V) [19]. Calculations reveal that combined with energy filtering, this leads to more than an order-of-magnitude improvement in energy-filtered sources used in advanced electron microscopes [19].

Here, we describe a different geometrical situation with a monocrystalline Nb field emitter with a radius of 23 nm and without a NP on the apex. In the following, we term this an Nb tip, in contrast to the NPT. The absence of the NP changes the associated geometry-dependent electronic band structure, leading to significant variations in the emission energy spectrum and the beam-current behavior compared to a NPT. In Sec. II A, we describe in detail the Nb tip and NPT fabrication by electrochemical etching and focused-ion-beam (FIB) ion milling, followed by annealing steps. Then, in Sec. II B, we present our field-emitter test and characterization setup and provide in Sec. III a theoretical analysis of the Nb-tip and NPT field-emission process. In Sec. IV, we give examples of the energy spectra for Nb-tip field emission at room or liquid-helium temperatures and compare them to the spectrum of a NPT. The beam current at different Nb tip voltages is described and we provide a beam-stability analysis over several hours. The Nb-tip emission tends to be less prone to adatom-related fluctuations than for a NPT and fits the Fowler-Nordheim (FN) theory [25,26] well, as do most commercial field emitters in microscopy. However, at low temperatures, the measured field-emission energy distribution is still significantly more monochromatic than conventional electron-beam sources, with around 110-meV FWHM. This can be sufficiently narrow for several techniques in electron microscopy and spectroscopy. By determining the temperature dependence of the field-emission spectra, we can demonstrate, for a Nb tip and a NPT, that the energy width changes only moderately between liquid-helium and liquid-nitrogen temperatures. This is of relevance for technical and commercial applications of our source.

We furthermore demonstrate that a layer of xenon adatoms on the Nb tip can increase the field emission by 2 orders of magnitude while not significantly changing the energy distribution. Finally, we discuss the role of superconductivity in the emission characteristics. There has been speculation [27]—and there have been theoretical predictions [28]—to the effect that electrons connected as a Cooper pair inside the superconducting tip may get emitted into vacuum in a correlated or even entangled state with opposite momentum and spin. We measure the two-electron correlation with nanosecond resolution and cannot confirm this phenomenon. However, we point out in Sec. V that this could be due to Nottingham heating [23,29–31], where the tip is locally heated due to the energy difference between the emitted electrons and the succeeding bulk electrons. This may cause the nanoscopic beam exit area on the tip apex to surpass the superconducting transition temperature. We discuss options to reverse this effect, leading to Nottingham cooling [21] and potentially realizing a correlated electron field emitter. Such an entangled electron source could have a significant impact on spectroscopy and quantum information science. Our observations are compared with previous field-emission studies on superconducting tips [27,32–36].

The Nb-tip electron-beam source presented in this paper hopefully opens up a promising field in high-resolution spectroscopy, limits the effect of aberrations, and may improves electron-energy-loss spectroscopy (EELS). It may decreases the impact of chromatic aberrations in low-voltage scanning electron microscopes and when combined with a monochromator, it may has the potential to enhance the energy resolution to the 1-meV level.

II. EXPERIMENTAL SETUP

A. Tip preparation

We fabricate the monocrystalline Nb tip shown in Fig. 1(f) in a four-step procedure. In case a NP should be generated on the apex, such as in Ref. [19], a fifth step is added. In most of the literature on Nb field emitters, polycrystalline wires have been used as a base for tip fabrication [27,35–37]. Only two studies have prepared a monocrystalline Nb source. One of them has realized a [111] tip by electrochemical polishing from a single-crystal wire and has measured the room-temperature energy distribution [38]. The other study has not prepared a tip but has analyzed the field-emission current from crystalline Nb surfaces at high voltages at room temperature [39]. For the generation of a beam with a narrow energy distribution, a monocrystalline structure is believed to be preferred, since the ratio between the electrical resistance at room temperature compared to 4.2 K depends on the crystalline quality and is significantly higher for monocrystalline wires [35,40].

Our tip preparation starts with a larger Nb [100]-oriented single crystal with a purity of 4N+ that is cut into rectangular monocrystalline pieces of

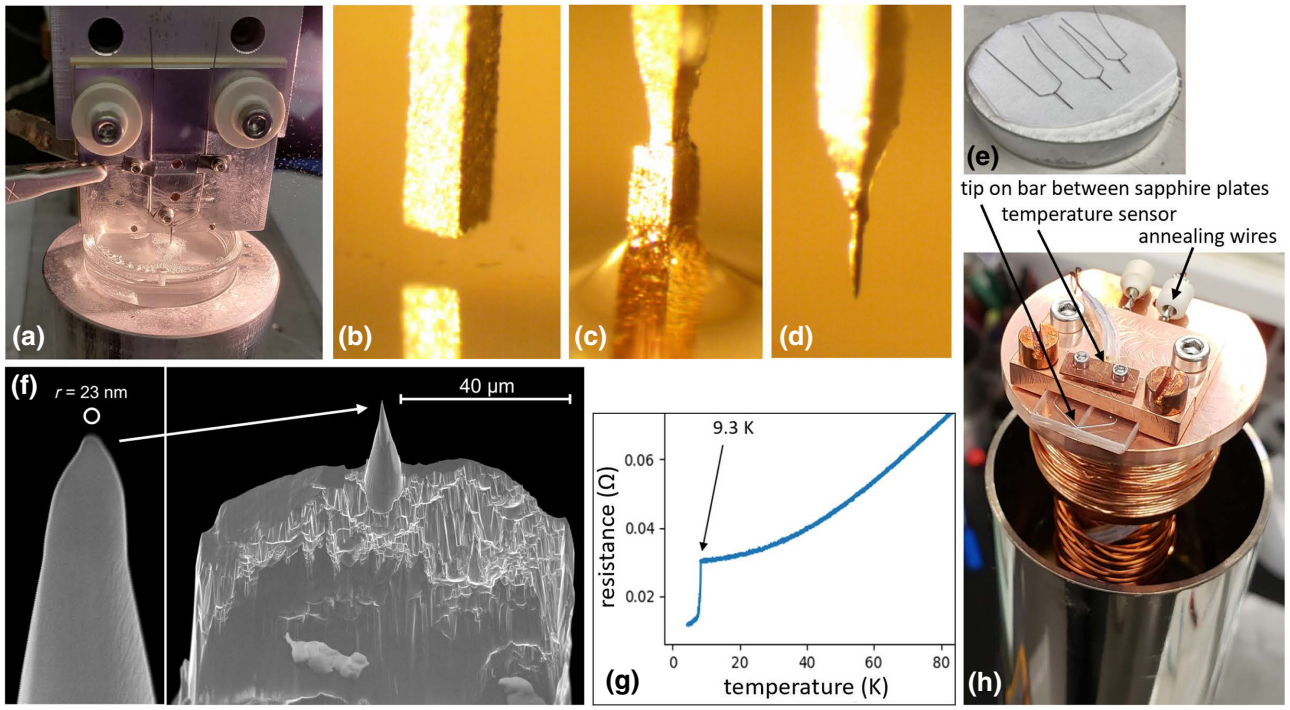

FIG. 1. Tip fabrication. (a) The setup for the electrochemical etching of the monocrystalline niobium tip that is spot welded on a cathode holder and submerged in a KOH solution. (b)–(d) A single crystal rectangular Nb wire (b) before etching, (c) during etching, and (d) after etching. (e) Monocrystalline Nb wires spot welded on a V-shaped bar before etching. (f) The tip after ion milling in the FIB: enlarged views of (left) the apex and (right) the tip on the shaft. (g) The four-point measurement of the resistivity of the bar wire versus the tip temperature, with the superconducting transition step at 9.3 K. (h) The cryostat head positioned upside down without the cooling shield, indicating the tip mounting between two sapphire plates.

$0.25 \times 0.25 \times 10$ mm, as shown in Fig. 1(b), by electrical-discharge machining (EDM, Surface Preparation Laboratory B.V). One of these pieces is then spot welded onto a polycrystalline Nb wire bar with the same diameter (0.25 mm) and bent to the V-shaped form as visible in Fig. 1(e). In the next step, the monocrystalline piece is etched to a tip based on a procedure described in Ref. [37] and with the setup illustrated in Fig. 1(a). The monocrystalline wire on the bar is cleaned with isopropanol, acetone, and demineralized water in an ultrasonic bath. It is clamped on a holder that serves as an anode and immersed in a 5 M potassium hydroxide (KOH) solution for electrochemical etching. A graphite electrode placed in the solution serves as the cathode [not visible in Fig. 1(a)]. The immersion depth of the niobium wire should be approximately 2 mm and is set by a micrometer stage and monitored by an optical microscope using a camera. The etching process starts by applying a 50-Hz 20-V_{pp} ac voltage between the cathode and anode. At the surface, a neck forms, narrowing the wire until the lower part (in the solution) falls off after about 20 min. More KOH solution is constantly added during etching to compensate for evaporation and to keep the neck at the surface of the liquid. This creates the approximately 80-µm-diameter tip shaft, visible in Fig. 1(f), which serves as a base for ion-beam milling. For the fabrication of sharper tips, pulse-wave-form etching, as described in Ref. [37], can be applied. Figures 1(b)–1(d) show the tip before, during, and after the etching process, respectively. Finally, the tip is cleaned by immersing it in isopropanol and deionized water and stored in vacuum or a dry gas atmosphere to avoid oxidation.

In the fourth step, the tip is then further shaped by gallium ion-beam milling in a FIB (Thermo Fisher Scientific, model FEI Helios G4 UX). We mill along the longitudinal axis with an annular pattern to cut the base symmetrically and form a conical Nb tip. The tip is imaged by SEM in the same instrument, as shown in two magnifications in Fig. 1(f). The left image, at high magnification, indicates a tip radius of approximately 23 nm. After this procedure, the tip is removed from the FIB and installed on a closed-cycle liquid-helium cryostat (Advanced Research Systems, model DE-210). Figure 1(h) illustrates that it is mounted between two sapphire plates, allowing electrical isolation and thermal conductivity. It is further thermally isolated by a copper cooling shield with a small aperture for the beam path, which is removed for the picture in Fig. 1(h). We confirm superconducting conditions by cooling the tip to 5.2 K, which is well below the transition temperature of Nb ($T_c = 9.3$ K), and perform a four-point resistivity measurement while the temperature of the cryostat increases.

The expected step in resistivity at T_c can be clearly observed in Fig. 1(g) and is further used for temperature calibration.

A stable and intensive field emission requires stringent surface cleaning and ultrahigh-vacuum conditions. In Refs. [27,35,36], the Nb tip is prepared with repeated surface cleaning by field evaporation with a high voltage of +6 kV. Here, we clean the tip by annealing to approximately 1220 K, where the tip is clearly glowing. The annealing is done, while the cryostat is still on, by ramping up a current of 4.85 A through the polycrystalline Nb wire bar. To avoid the tip getting blunt, an electrical bias of −3 kV is set on the extractor aperture during the process. The temperature is monitored through a vacuum window by a disappearing-filament pyrometer and the procedure is repeated several times. The tip geometry can vary depending on the annealing duration, ramping speed, temperature, and number of heating cycles. This results in either a Nb tip with an approximately 23-nm radius or, as described in detail in Refs. [19,37], in the formation of a NPT with a nanoprotrusion smaller than 5 nm [19,20] on the tip apex. We automate the annealing process with a programmable current source and can form the desired geometry in most of the cases. Sometimes, there are still differences in the outcome, altering the emission properties of the tip after a certain annealing cycle. This changes the onset voltage of the field emission, which is observed anywhere between $V_{\text{tip}} = -300$ V and $V_{\text{tip}} = -500$ V.

B. Field-emitter characterization setup

The setup to measure the field-emitter properties is illustrated in Fig. 2. The vacuum pressure needs to be extremely low during the cleaning procedure [27] and the field emission. Thus, the base pressure in our setup is kept at approximately 8×10^{-11} Torr by a large non evaporable getter (NEG) pump in combination with a turbo pump. The chamber contains the closed-cycle liquid-helium cryostat with a heater element for temperature control of the Nb tip between 5.2 and 82 K. The cryostat is placed on a rotational flange and a three-dimensional manipulator, so that the tip can be rotated and pointed toward three ports for measuring different beam features without breaking the vacuum. The first one is a hemispherical electron-energy analyzer (ScientaOmicron DA20 R) with a resolution of 3 meV. For field extraction and beam guiding, an extractor aperture and a custom deflector element are installed between the tip and the entrance and collection optics of the analyzer. A cryostat rotation by 45° points the tip toward a Faraday cup (Kimball Physics, FC-71) with a picoamperemeter (Keithley, Model 237). This allows recording of the FN plots of the beam current as a function of the applied tip voltage. Additionally, it can perform long-term emission-stability measurements. After a 90° rotation, the emitter can be pointed toward a single-electron delay-line detector (RoentDek DLD HEX100) with a high spatial and temporal resolution. This allows imaging of the beam profile with the angular distribution at low intensity. Along the beam path, a custom Einzel lens for beam magnification is positioned, followed by a deflector for alignment. This spreads the emission across a large area on the MCP, which is necessary to determine spatial and temporal electron-electron correlations on the nanosecond scale.

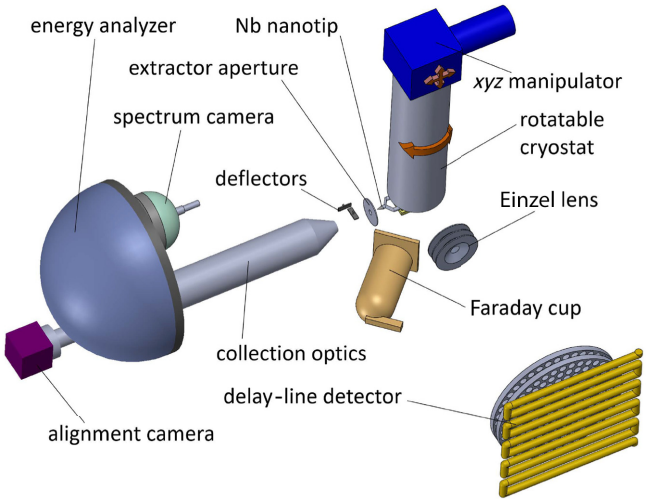

FIG. 2. A sketch of the experimental setup for the in-vacuum characterization of the cryogenic niobium field emitter. It allows measurement of the beam energy distribution, the emission current, the angular profile, and the electron-electron correlations.

III. THEORY

The electrons in a metallic cathode are kept from escaping to vacuum by the work function ϕ, an electrostatic barrier above the Fermi level E_F. This potential barrier can be decreased by a negative bias voltage applied to the cathode or a positive bias on the extraction aperture. It gets further decreased by the image-charge potential due to the interaction of the beam electrons with the conduction electrons in the metal:

$$V_{\text{pot}}(x) = \phi - eFx - \frac{e^2}{16\pi\epsilon_0 x}, \tag{1}$$

where $F = |\mathbf{E}| = \beta V_{\text{tip}}$ is the magnitude of the electric field at the emission region, with $\beta \approx 0.008$ nm^{-1} being an enhancement factor that is a function of the geometry of the tip at an applied tip voltage V_{tip} [41]. The total energy distribution, with respect to E_F, of electrons emitted from a finite-temperature metallic tip cathode in the Murphy-Good regime between pure field emission and thermal emission can be written as

$$G(E,F,T,\phi) = \frac{4\pi m f\,(E,T) D(F,\phi)\exp(E/D(F,\phi))}{h^3 \exp(B(F,\phi)\phi^{3/2}/F)}, \tag{2}$$

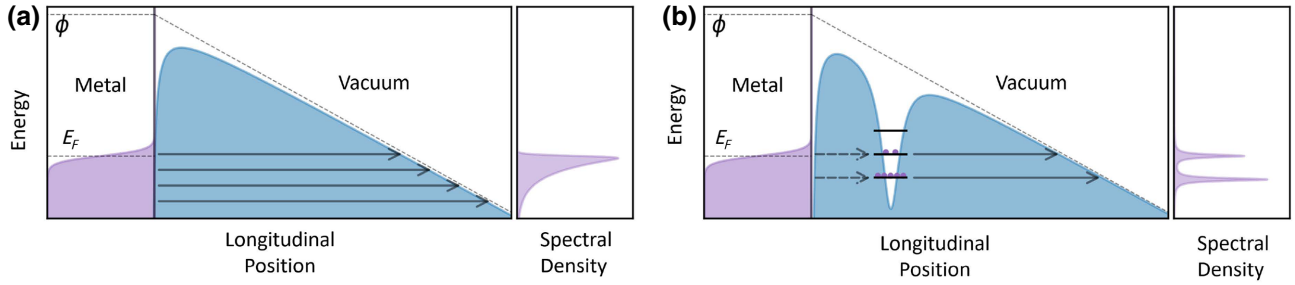

FIG. 3. (a) An illustration of the FN field-emission process from a Nb tip that is set on a high voltage. The electrons tunnel through the Coulomb barrier from states around the Fermi energy E_F into vacuum. The inset on the right indicates the single broad energy peak in the spectra that is highly asymmetric due to the sharp cutoff at E_F at low temperatures. (b) The emission process from a NPT, where quantum band states form in the NP, acting as intermediate levels in the Coulomb barrier. The associated peaks in the field-emission energy spectrum are Lorentzian distributed with significantly smaller widths. They can be shifted relative to E_F by the applied tip voltage.

where T is the temperature, $f\,(E,T)=(1+\exp(E/k_BT))^{-1}$ is the Fermi-Dirac distribution, $B(F,\phi)=8\pi\sqrt{2m}v(y)/3h$ and $D(F,\phi)=e\hbar F/2\sqrt{2m\phi}$ with $v(y)\approx 1-y^2(3-\ln(y))/3$ and $y=\sqrt{e^3F/4\pi\epsilon_0\phi^2}$ [26]. The tunnel barrier increases linearly in E_F-E with $E\ll\phi$, resulting in an exponentially decaying emission probability below E_F. There is a hard cutoff in the emission probability above E_F due to the sharp exponential tail of the Fermi-Dirac distribution at low temperatures. This is illustrated in Fig. 3(a). Integration over G and multiplication by the electron charge e gives the well-known FN current density, $J(F,T,\phi)=e\int dE\,G(E,F,T,\phi)$ [42]. As shown in Fig. 4, the width of the FN energy distribution from standard emitters is limited. Depending on the emitting area (the blue, orange, and green lines in Fig. 4 for emission radii of $r_{tip}=5$, 25, and 100 nm, respectively) the FWHM energy distribution for the nanoampere beam currents that are usually required for electron microscopy is in the range of 100 meV at $T=0$ K.

However, for a significantly smaller field-emission energy distribution at a comparable beam current, a different emission process needs to be established that leverages distinct quantum states due to the surface geometry of extremely sharp tips. Equation (2) can be used to model the total energy distribution and current density from tip emitters with tip radii down to a single-atom tip. But if the height-to-width ratio of the tip exceeds some critical threshold, such as in the NPT, the confinement potential creates localized discrete electronic states away from the bulk Fermi sea. These states are commonly approximated as a well in the Coulomb barrier, spatially separated from, yet supplied directly by, the Fermi sea [20], as illustrated in Fig. 3(b). The discrete states of the NP act as an intermediary between the Fermi sea and vacuum, giving a resonant enhancement of the tunneling probability at the energy of the midbarrier state; a process resembling the physics of single-atom resonance-tunneling spectroscopy [43]. If we neglect the interference between the direct and resonant tunneling amplitudes, the NPT emission total energy distribution can be written as

$$G_{\rm tot}(E,F,T,\phi)\approx G(E,F,T,\phi)\left(1+\sum_n R_n(E,F)\right), \tag{3}$$

where the resonant-enhancement factors, R_n, have the form

$$R_n(E,F)=\frac{A_n}{(E-E_n+\alpha F)^2+\Gamma_n^2}, \tag{4}$$

i.e., have a Lorentzian shape centered at the midbarrier state energy E_n that shifts in energy proportionally with the applied field, an associated line width of Γ_n, and a resonance magnitude of A_n [43]. They are single-peaked functions corresponding to each discrete state of the NP at an energy that shifts linearly with the electric field strength

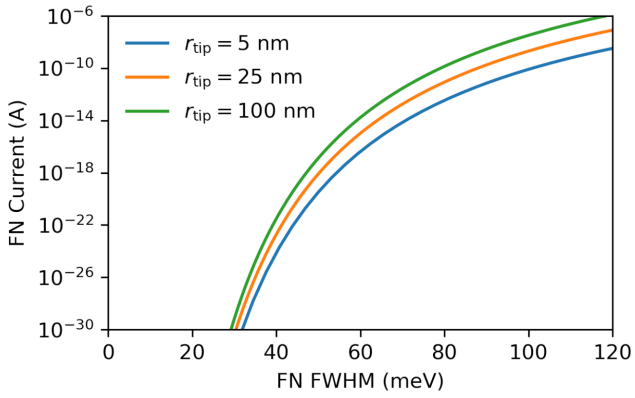

FIG. 4. The dependence of the electron-beam current as a function of the energy distribution FWHM for three standard field emitters that can be described by the FN relation with different radii of their emitting areas at $T=0$ K. Reasonable currents for microscopy applications in the nanoampere regime lead to energy widths around 100 meV.

at the tip. With increasing field strength F, the Coulomb barrier to vacuum is lowered, shifting the NPT field emission peaks down in energy with respect to E_F. As these resonances are multiplied by the envelope of FN emission, resonant tunneling is most efficient through states near E_F and the applied field required for resonant tunneling can be much lower than is typically necessary for a tip without a NP. Consequently, resonant emission from a discrete NPT state can be present without the FN emission with the broad energy spectrum and NPT emission can be realized with line widths in the order of tens of millielectronvolts [19,22]. Extremely narrow field-emission energy-spectrum peaks can be achieved when the tip is cold enough that the width of the Fermi-Dirac distribution is narrower than the line width of the discrete state and the center energy is near E_F. Then, the peak shift with the applied field can be used to adjust the emission peak such that the Fermi edge of the distribution cuts off a portion of the peak, lowering the line width of the total energy distribution of the emission [19,21]. We demonstrate this process using the setup described in Ref. [19]. The physics of this observation is similar to an early method in atomic spectroscopy for atoms adsorbed to metallic surfaces [43] and similar resonant field-emission spectra have been demonstrated with gold nanoclusters deposited on tips [44], single-atom nanoprotrusions grown *in situ* on tips by high field and heat [45], edge states from graphene on tips [46], and photoassisted emission from a quantum dot on a tip [47]. It has been shown that the exact energy distribution of emission from nanoprotrusions can be determined by density-functional calculations [24]. However, there is a strong dependence on the exact geometry of the apex and uncertainty in the growth process [45]. Thus, it can be more useful to take an empirical approach and assume a resonant enhancement factor that is similar to resonant tunneling through an adsorbed surface atom [21]. This has been derived rigorously for a deposited gold cluster in Ref. [48].

IV. RESULTS

We describe the field emission of the Nb tip shown in Fig. 1(f) without a NP in a superconducting state at 5.2 K and compare it with a NPT. The upper blue curve in Fig. 5 presents the energy spectrum of the Nb tip (without NP) field emission at room temperature and at a tip voltage of $V_{\text{tip}} = -600$ V, with a FWHM of 185 meV. As expected from the FN theory, it is significantly broader than the emission from the same tip at 5.2 K, with a FWHM of 75 meV (orange middle curve). After a NP is formed on the apex of the tip by the annealing procedure described in Sec. II A, the NPT is cooled again to 5.2 K and yields an energy distribution with an ultranarrow FWHM of 22 meV (green lower curve), also at $V_{\text{tip}} = -600$ V. As expected, the peak is Lorentzian shaped and is cut off by

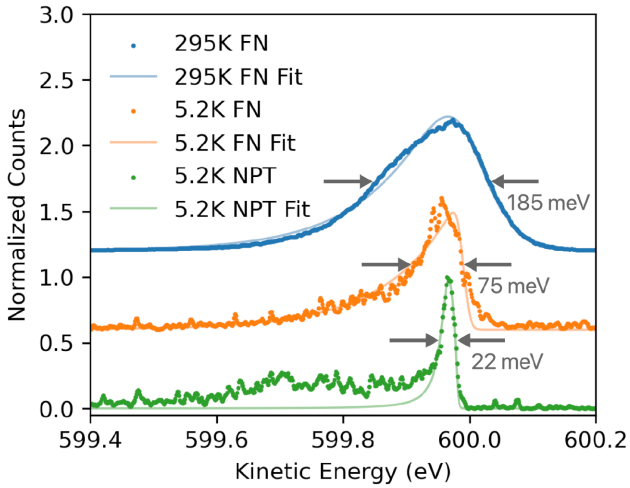

FIG. 5. A comparison of the Nb-tip field-emission energy distribution at the Fermi edge without a NP at room temperature (blue upper curve), at a superconducting temperature of 5.2 K (orange middle curve), and after the formation of a NP on the tip apex also at 5.2 K (green lower curve).

the sharp low-temperature Fermi edge. Our measurements indicate clearly that the temperature reduction decreases the energy width of the FN emission of the Nb tip significantly. Further decrease is feasible by changing the tip apex geometry by adding the NP, as described in Sec. III. The field-emission energy spectrum, brightness, and current stability of a NPT are discussed in detail in Ref. [19]. There, a different monocrystalline Nb tip has been used but both emitters have been fabricated according to the same procedure as described above.

For further beam analysis of the superconducting Nb tip without the NP at 5.2 K, we perform a measurement of the FN current versus the tip voltage with the Faraday cup indicated in Fig. 2. As is already observed in the room temperature energy spectra in Fig. 5, the field emission follows the described FN current density $J(F, T, \phi)$. A Faraday-cup measurement is expected to give a linear relationship between the natural log of emitted current divided by the square of the tip voltage as a function of the inverse tip voltage [25]. This is perfectly reflected in our Faraday measurement, shown in Fig. 6, for a Nb-tip field emission at a temperature of 5.2 K, where the data points can be well matched by a FN fit function. The observed emission is in clear contrast to such a measurement for the Nb tip with a nanoprotrusion at the apex, in Ref. [19]. There, we determine a clear deviation from the FN theory for the ultranarrow discrete state emission.

Furthermore, we perform a long-time field-emission current-stability measurement at 5.2 K, monitoring the beam current over 5 h with the Faraday cup for the Nb tip (without the nanoprotrusion). The data are shown in Fig. 7. The closed-cycle cryostat pumps liquid helium with

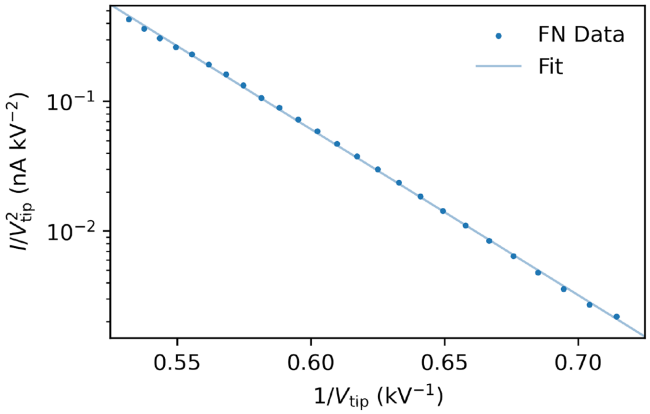

FIG. 6. The FN measurement with the Faraday cup of the field-emission current versus the applied tip voltage for the superconducting monocrystalline Nb tip shown in Fig. 1(f). The data matches well with a linear FN fit function.

a period of 1.5 s, which causes the tip to be mechanically displaced by about 50–100 μm in every pump cycle relative to the fixed extraction aperture. This movement changes the field configuration throughout the pump cycle, causing slight deviations in the field-emission current, as can be observed in the blue measurement points of Fig. 7. We carry out a Fourier analysis of the data for an emission current of around 1.1 nA and remove the fluctuations due to the periodic vibration frequency of the cryostat, leading to the orange dots in Fig. 7. For the long-time stability, drifts and jumps of the cryotip beam current, which are also known from cold field emitters made of other materials, play a more important role. This can also be observed in Fig. 7, particularly after 3 h, when adatom accumulation on the surface increases. We measure long-time fluctuations on the order of 10% of the mean tip current.

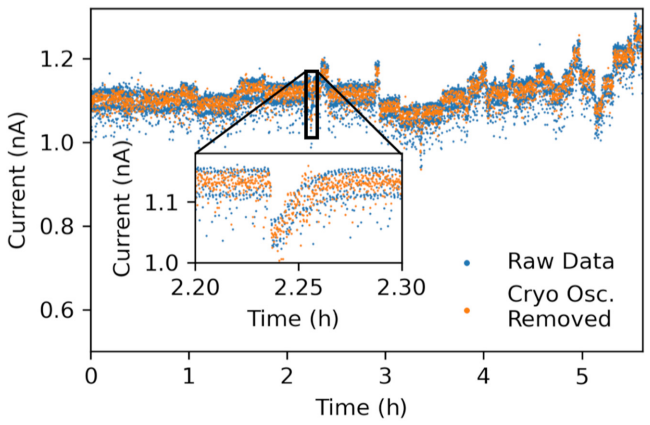

FIG. 7. The stability measurement of the superconducting Nb-tip field-emitter beam current (blue points). The orange points represent the data after a Fourier filter to remove the periodic current fluctuations from the closed-cycle cryostat pumping vibrations (cyro osc.).

The introduction of xenon (Xe) gas to the vacuum chamber with Nb-tip field emitters at cryogenic temperatures has been shown to increase the emission current significantly [37]. This is due to the adsorption of the Xe atoms onto the tip surface, which is known to lower the effective work function [37]. We carry out similar studies with our superconducting emitters and set a sequence of Xe gas exposures to the Nb tip at a temperature of 5.6 K. Every step increases the Xe adsorption by approximately 0.5 L (1 Langmuir(L) $= 10^{-6}$ Torr s). Then, we determine the field-emission total count rate of the magnified angular distribution with the delay-line detector at a constant tip voltage of −1150 V. The data are shown in Fig. 8(a), revealing an increase in the count rate by a factor of 116 at a Xe exposure of 14 L. While the field strength and tip geometry have long been used as parameters to tune the emission properties of field emitters, working with a cryostat for temperature control and adsorbed gases for work-function lowering significantly expands the parameter space for tunable emitters. We also analyze if the Xe coverage changes the energy distribution of the beam. As demonstrated in Fig. 8(b), the field-emission energy FWHM of the clean tip is 69 meV. After 14 L Xe-gas coverage, the FWHM is 66 meV. The difference is within our

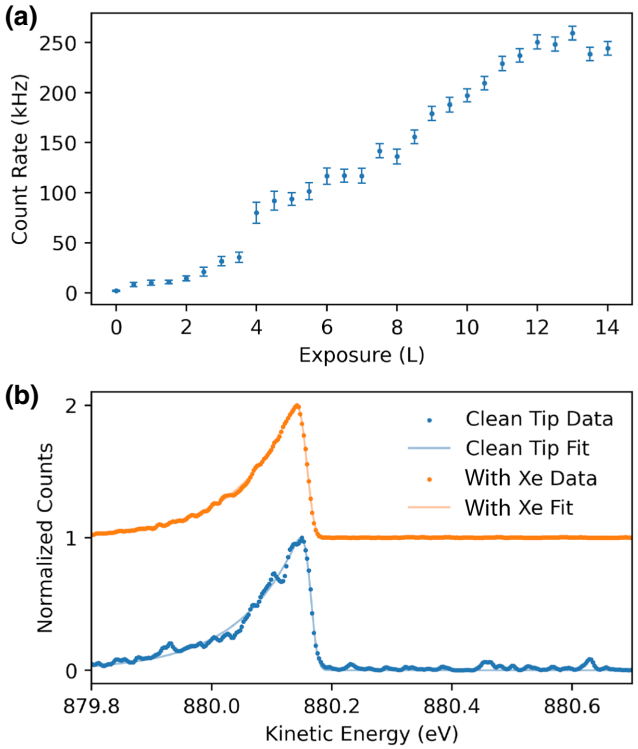

FIG. 8. (a) The increasing beam current with increasing coverage of xenon gas adsorbed on the superconducting Nb tip at a constant field-emission voltage. (b) Energy spectra with a xenon coverage of 14 L on the Nb tip (top orange curve) and for the clean Nb tip (lower blue curve), both with a FN fit.

measurement error and both energy peaks are distributed according to FN, so we do not observe any change in the beam energy distribution after Xe-atom adsorption on the tip.

As a next step, the temperature dependence of the field-emission energy spectrum of our electron source is measured. Previous studies have determined the beam energy width of cold platinum-tip field emission from localized surface band states as ranging from 80 K to 293 K [22]. They have demonstrated an energy distribution of 64 meV at 80 K and found a linear increase in the line width up to 100 meV at 293 K. Considering their calculated instrument broadening, it has been predicted that the energy distribution could be decreased to around 20 meV by lowering the temperature close to 0 K [22]. In Ref. [19] and Fig. 5 of this work, we can demonstrate this predicted ultranarrow energy width with the Nb nanoemitters with a nanoprotrusion. Here, we compare the temperature dependence between 5.6 K and 82 K in Fig. 9 for the two described tip-geometry configurations. The blue dots and the blue FN fit in Fig. 9(a) illustrate the measured temperature dependence of the FWHM of the energy distribution of the beam for the Nb tip that follows the FN description. The orange dots with a linear fit exhibit the temperature-dependence FWHM data of the resonant localized band state emission for the NPT (fabricated in Ref. [19]). The results reveal that there is only a moderate broadening in the line-width FWHM from liquid-helium (4.2 K) to liquid-nitrogen (77 K) temperatures. This observation is quite significant for the integration of this field emitter in electron microscopes, since it is technically much easier and cheaper to cool the emitter with liquid nitrogen. The outcome demonstrates that narrow energy distribution emission well below 40 meV is feasible at liquid-nitrogen cooling. The data also indicate a difference in energy width of approximately 75 meV between the two tip geometries.

Another important question to address is the possible correlation between electrons emitted from the superconducting tip. According to a theory paper by Yuasa *et al.* [28], a niobium tip is a possible source of entangled free electrons with opposite spin and momentum following field emission of correlated Cooper pairs. However, it is still an open experimental question if a correlated two-electron emission can be realized from solid-state surfaces to the vacuum. Solid-state Cooper-pair tunneling through a barrier is well known in physics, e.g., it is the basis for superconducting quantum interference devices (SQUIDs) and it is applied in superconducting scanning-tunneling experiments [49]. Also, a recent solid-state experiment has demonstrated efficient Cooper-pair splitting into normal conductors in nanostructured devices [50], resulting in spatially separated pairs of entangled electrons. A further theoretical study has considered a superconducting tip in a high electric field [51] and predicted the existence of vortices and superconducting states that persist in nanosized tips up to fields much larger than the bulk critical field. They conclude that a significant Cooper-pair density is present even in the confined space of a tip with a size on the order of the coherence length. The confirmation of entangled electron emission from a superconducting source would be a breakthrough in the field. Such an emitter would create significant opportunities for quantum information science with free electrons, by analogy with the scientific impact of entangled two-photon sources [52]. They have led to major achievements in quantum optics, including the violation of Bell inequality [53], quantum cryptography [54], quantum teleportation [55], and quantum computing [56]. It would additionally

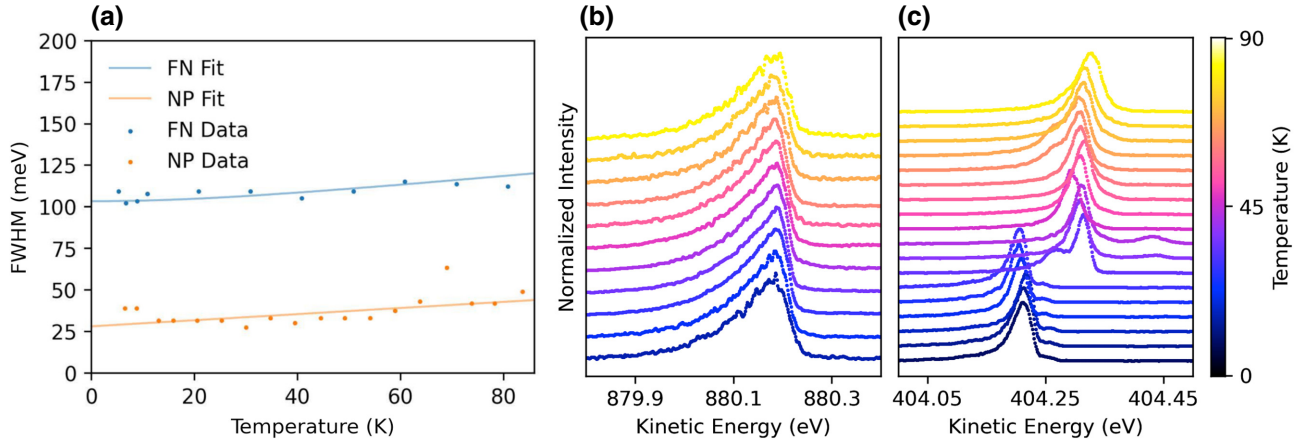

FIG. 9. (a) The temperature dependence of the electron energy distribution FWHM in the beam from a Nb-tip field emitter with (orange dots) and without (blue dots) a nanoprotrusion on the apex. The blue line is a fit according to the FN theory including instrument noise and the orange line is a basic linear fit. (b) Temperature-dependent FN emission spectra corresponding to the blue dots in (a). (c) Temperature-dependent nanoprotrusion emission spectra corresponding to the orange dots in (a). The origin of the sudden shift at approximately 25 K by approximately 10 meV is unknown.

allow correlated two-electron spectroscopy, with an exceptional accuracy that depends on the extremely low energy difference between the correlated electrons compared to the energy variation between single electrons in an uncorrelated beam.

For that reason, we perform an electron correlation analysis in the field emission of our Nb emitter. The delay-line detector in our setup (see Fig. 2) is capable of verifying electron-pair emission with high spatial and temporal resolution if the electrons are spatially separated by more than approximately 8 mm [57]. Based on the predicted opposite initial momentum of the correlated electrons [28], they are expected to arrive at the detector with a distinct distance *dr* within a few nanoseconds *dt*. To increase the local separation, the beam gets magnified by the Einzel lens across the delay-line-detector area with a radius of 50 mm. The results are shown in Figs. 10(a) and 10(b) for the superconducting tip temperature of 5.6 K and in Figs. 10(c) and 10(d) for a normal-conducting tip temperature of 44 K. In both cases, we integrate over 7×10^5 counts. Figures 10(a) and 10(c) are the magnified angular beam profiles at normal and superconducting temperatures as they arrive at the detector, respectively. In Figs. 10(b) and 10(d), we add the arrival-time information to plot the time difference *dt* between any two detected electrons up to 30 ns against their spatial distance on the detector *dr*. It provides the correlated events under superconducting [Fig. 10(b)] and normal-conducting [Fig. 10(d)] conditions. There is no significant difference between the two measurements. The counts in the lower right corner with $dr \sim 0$ mm and $dt \sim 20$–30 ns are believed to be due to ion feedback in the detector, where a residual gas atom in an MCP channel gets ionized by an electron avalanche and accelerated in the opposite direction. Within the same channel, it triggers a second delayed electron pulse. This is a known effect for MCP detectors. The origin of the diagonal features in Figs. 10(b) and 10(d) is not clear; we assume double counts due to ringing effects in the detector electronics. However, these are only a few seemingly correlated counts in both images relative to the total accumulated signal. They are extremely rare and their number and pattern are about the same at normal and superconducting temperature. For that reason, we do not observe any significant two-electron correlation in the superconducting field emission.

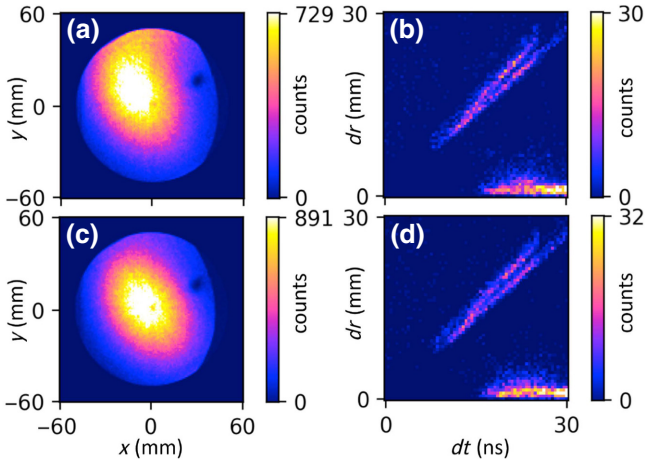

FIG. 10. (a) The integrated total electron-beam signal on the delay-line detector at a superconducting tip temperature of 5.6 K. (b) A correlation analysis between two consecutive electrons with the time difference *dt* and the spatial separation *dr* at a superconducting tip temperature corresponding to (a). (c) The integrated signal and (d) the correlated counts at a normal-conducting temperature of 44 K.

V. DISCUSSION AND CONCLUSIONS

We discuss the field-emission properties of monocrystalline niobium-tip electron-beam sources at a temperature of 5.2 K well below the superconducting transition. This work complements our recent publication [19], where we emphasize the resonant emission through band states with ultralow energy distribution from a Nb nanotip with a nanoprotrusion on the apex. Here, we concentrate on the emission behavior of such an Nb tip without the nanoprotrusion and compare the two cases with each other. We provide a detailed description of the fabrication steps to produce a tip with a 23-nm radius. The tip is cooled by a liquid-helium cryostat. Energy distributions around 100 meV are measured, with an emission-current stability of 10% in the nanoampere regime. The current increases with the tip voltage according to the FN description. Additionally, it is demonstrated that the adsorption of xenon atoms leads to an increase in the beam intensity by 2 orders of magnitude.

We also compare the temperature behavior of the field emission for both emission processes from 5.6 K to approximately 82 K. It is observed that the energy width of the beam does not change strongly between liquid-helium and liquid-nitrogen cooling temperatures. With the NPT, narrow energy widths below 40 meV are observed and with the Nb tip, they remain below 110 meV. The cooling with liquid-nitrogen eases the commercial application of this source significantly compared to the use of liquid helium. According to an evaluation based on BCS theory by Gadzuk [35,58], a narrow peak with an energy width below 0.1 meV is expected to be observed at the Fermi edge (E_F). In Refs. [35,36], a 20-meV peak has been claimed to appear near E_F only at superconducting temperatures. However, we do not measure such distinct changes around T_c.

Furthermore, electron-electron correlation measurements are performed, resulting in no evidence of two-electron field emission from the superconducting tip, as predicted by theory [28]. This result is potentially due

to two reasons. Either there is no correlated electron-pair emission from the superconducting state around the Fermi energy E_F or there is local heating at the beam-exit area of the electrons, leading to nonsuperconducting conditions even at a measured overall tip temperature below T_c. A local heating mechanism that may need to be considered is Nottingham heating [23,29–31]. The high current from a small spatial area can thereby induce localized heating that can even destabilize the structural integrity of the apex [59]. This is due to the Nottingham effect in which electrons emitted from below E_F are, on average, colder than the electrons in the Fermi sea. This results in net heating, because most electrons that tunnel through the Coulomb barrier are lower than E_F at cryogenic tip temperatures [29,31]. The effect has been measured by Binh *et al.* [23] for a tungsten tip with a single-atom protrusion. They have observed no heating below 0.3 pA but a local change in temperature of approximately 30 K at a beam current of 9 pA with a linear increment in between. Our count rate in Fig. 10 is in the femtoampere regime and therefore significantly smaller. However, superconductors are considered to be bad thermal conductors, so our situation is potentially not comparable to normal-conducting tungsten tips at these cryogenic temperatures. This will be a matter for future investigations.

It is worth noting that the effect can be reversed if the emission mostly comes from energies above E_F, causing Nottingham cooling [21]. This could, in principle, be realized with a NPT by shifting the surface resonant peaks slightly above E_F by lowering the extraction voltage [19,21]. It is challenging to actually cool efficiently at cryogenic temperatures, since there are not many electrons left above E_F that can be addressed by the resonance peak. But with the possibility of precisely shifting an ultranarrow Lorentzian excitation that is truncated at E_F, such as we observe in Fig. 5 and in Ref. [19], a stable condition may be found that allows local Nottingham cooling and possibly correlated electron emission. This may lead to the predicted correlated and entangled two-electron emitter [28]. Alternatively, tips made from materials with a higher superconducting transition temperature could be applied, e.g., niobium nitrite [60]. Such sources could become an electron-optical analog to the parametric down-conversion two-photon source in quantum optics [52] and open up unique modes in quantum information science, quantum metrology, and electron spectroscopy. They could also play an important role in quantum correlation measurements in electron microscopy, such as free-electron entanglement with optical excitations, e.g., plasmon polaritons [61]. It is not clear to what extent the Coulomb repulsion would influence such a correlated source. In Ref. [28], the entangled superconducting electron emission has been predicted while explicitly neglecting the Coulomb interaction between the emitted electrons, considering the low current densities in emission experiments from superconducting tips [36]. However, this is only valid for stochastic electron emission where, at low count rates, most subsequent electrons have a significant time separation. For that reason, it is a question of space-time confinement of the correlated emission. This has been studied in recent experiments about emission from a tungsten nanotip [62] or a ZrO/W Schottky [63] emitter induced by a femtosecond laser pulse. The authors have reported a two-electron emission that is highly anticorrelated in energy due to dynamic Coulomb repulsion. Such preparation of highly non-Poissonian electron beams is of great relevance in microscopy, lithography, and quantum electron optics. It has revealed a mean energy splitting of a few electronvolts and a correlation decay time in the order of 100 fs. For that reason, it can be assumed that a two-electron emission process from the superconductor within this time difference will be influenced by the Coulomb interaction. Further clarification in future studies is required to analyze the competition between superconductivity and Coulomb interactions [64] in low-dimensional systems such as a nanotip and how it will influence the field-emission process.

The near-monochromatic field emission of our superconducting Nb source is highly coherent. The longitudinal coherence length is inversely proportional to the width of the energy distribution and the transversal coherence is due to the small virtual source size. This is especially important in quantum applications with electron matter waves in, e.g., sensor technology [5,6], interferometry [12], quantum information science [7], multipass-transmission electron microscopy [65], and quantum electron microscopy [66,67].

Our source could be combined with a monochromator, which would lead to an extremely low electron-beam energy distribution on the millielectronvolt or even submillielectronvolt scale, while still maintaining reasonable beam currents for microscopy applications. A high-brightness free-electron source based on a Nb tip with a native-energy line width on the order of tens of millielectronvolts has a myriad of potential benefits throughout all electron microscopy and would open up several regimes, such as high-resolution EELS [68] including the direct imaging of vibrational modes [16], the analysis of semiconductor band gaps or defects, and low-loss structures in metal nanoparticles, solar cells, or organic materials. The reduction in the field-emitter energy distribution will also reduce chromatic aberrations, particularly in low-voltage scanning electron microscopes. This will improve their spatial resolution into the subnanometer range.

ACKNOWLEDGMENTS

Work at the Molecular Foundry was supported by the Office of Science, Office of Basic Energy Sciences, of the U.S. Department of Energy under Contract No.

DE-AC02-05CH11231. This material is based upon work supported by the U.S. Department of Energy, Small Business Innovation Research (SBIR)−Small Business Technology Transfer (STTR) program under Award No. DE-SC-0019675. We also acknowledge support by the Deutsche Forschungsgemeinschaft through research Grant No. STI 615/3-1.

[1] Q. Chen, C. Dwyer, G. Sheng, C. Zhu, X. Li, C. Zheng, and Y. Zhu, Imaging beam-sensitive materials by electron microscopy, Adv. Mater. **32**, 1907619 (2020).

[2] C. Ophus, Four-dimensional scanning transmission electron microscopy (4D-STEM): From scanning nanodiffraction to ptychography and beyond, Microsc. Microanal. **25**, 563 (2019).

[3] A. E. Turner, C. W. Johnson, P. Kruit, and B. J. McMorran, Interaction-Free Measurement with Electrons, Phys. Rev. Lett. **127**, 110401 (2021).

[4] N. Kerker, R. Röpke, L.-M. Steinert, A. Pooch, and A. Stibor, Quantum decoherence by Coulomb interaction, New J. Phys. **22**, 063039 (2020).

[5] A. Rembold, G. Schütz, R. Röpke, W.-T. Chang, I.-S. Hwang, A. Günther, and A. Stibor, Vibrational dephasing in matter-wave interferometers, New J. Phys. **19**, 033009 (2017).

[6] A. Pooch, M. Seidling, M. Layer, A. Rembold, and A. Stibor, A compact electron matter wave interferometer for sensor technology, Appl. Phys. Lett. **110**, 223108 (2017).

[7] R. Röpke, N. Kerker, and A. Stibor, Data transmission by quantum matter wave modulation, New J. Phys. **23**, 023038 (2021).

[8] A. Feist, N. Bach, N. Rubiano da Silva, T. Danz, M. Möller, K. E. Priebe, T. Domröse, J. G. Gatzmann, S. Rost, J. Schauss, S. Strauch, R. Bormann, M. Sivis, S. Schäfer, and C. Ropers, Ultrafast transmission electron microscopy using a laser-driven field emitter: Femtosecond resolution with a high coherence electron beam, Ultramicroscopy **176**, 63 (2017).

[9] D. Ehberger, J. Hammer, M. Eisele, M. Krüger, J. Noe, A. Högele, and P. Hommelhoff, Highly Coherent Electron Beam from a Laser-Triggered Tungsten Needle Tip, Phys. Rev. Lett. **114**, 227601 (2015).

[10] H.-S. Kuo, I.-S. Hwang, T.-Y. Fu, Y.-C. Lin, C.-C. Chang, and T. T. Tsong, Noble Metal/W(111) Single-Atom Tips and Their Field Electron and Ion Emission Characteristics, Jpn. J. Appl. Phys. **45**, 8972 (2006).

[11] C.-C. Chang, H.-S. Kuo, I.-S. Hwang, and T. T. Tsong, A fully coherent electron beam from a noble-metal covered W(111) single-atom emitter, Nanotechnology **20**, 115401 (2009).

[12] G. Schütz, A. Rembold, A. Pooch, S. Meier, P. Schneeweiss, A. Rauschenbeutel, A. Günther, W.-T. Chang, I.-S. Hwang, and A. Stibor, Biprism electron interferometry with a single atom tip source, Ultramicroscopy **141**, 9 (2014).

[13] N. De Jonge, Y. Lamy, K. Schoots, and T. H. Oosterkamp, High brightness electron beam from a multi-walled carbon nanotube, Nature **420**, 393 (2002).

[14] H. Zhang, Y. Jimbo, A. Niwata, A. Ikeda, A. Yasuhara, C. Ovidiu, K. Kimoto, T. Kasaya, H. T. Miyazaki, N. Tsujii, H. Wang, Y. Yamauchi, D. Fujita, S.-i. Kitamura, and M. Hironobu, High-endurance micro-engineered LaB_6 nanowire electron source for high-resolution electron microscopy, Nat. Nanotechnol. **17**, 21 (2022).

[15] S. Karkare, G. Adhikari, W. A. Schroeder, J. K. Nangoi, T. Arias, J. Maxson, and H. Padmore, Ultracold Electrons via Near-Threshold Photoemission from Single-Crystal Cu(100), Phys. Rev. Lett. **125**, 054801 (2020).

[16] O. L. Krivanek, T. C. Lovejoy, N. Dellby, T. Aoki, R. W. Carpenter, P. Rez, E. Soignard, J. Zhu, P. E. Batson, M. J. Lagos, R. F. Egerton, and P. A. Crozier, Vibrational spectroscopy in the electron microscope, Nature **514**, 209 (2014).

[17] E. Bauer, *Surface Microscopy with Low Energy Electrons* (Springer, New York, 2014), Vol. 23.

[18] H. W. Mook and P. Kruit, Construction and characterization of the fringe field monochromator for a field emission gun, Ultramicroscopy **81**, 129 (2000).

[19] C. W. Johnson, A. K. Schmid, M. Mankos, R. Röpke, N. Kerker, E. K. Wong, D. F. Ogletree, A. M. Minor, and A. Stibor, Near-Monochromatic Tuneable Cryogenic Niobium Electron Field Emitter, Phys. Rev. Lett. **129**, 244802 (2022).

[20] V. T. Binh, S. T. Purcell, N. Garcia, and J. Doglioni, Field-Emission Electron Spectroscopy of Single-Atom Tips, Phys. Rev. Lett. **69**, 2527 (1992).

[21] S. T. Purcell, V. T. Binh, N. Garcia, M. E. Lin, R. P. Andres, and R. Reifenberger, Field emission from narrow bands above the Fermi level of nanometer-scale objects, Phys. Rev. B **49**, 17259 (1994).

[22] S. T. Purcell, V. T. Binh, and N. Garcia, 64 meV measured energy dispersion from cold field emission nanotips, Appl. Phys. Lett. **67**, 436 (1995).

[23] V. T. Binh, S. T. Purcell, G. Gardet, and N. García, Local heating of single-atom protrusion tips during field electron emission, Surf. Sci. **279**, L197 (1992).

[24] Y. Gohda and S. Watanabe, Total Energy Distribution of Field-Emitted Electrons from Al(100) Surface with Single-Atom Terminated Protrusion, Phys. Rev. Lett. **87**, 177601 (2001).

[25] R. G. Forbes, A. Fischer, and M. S. Mousa, Improved approach to Fowler-Nordheim plot analysis, J. Vac. Sci. Technol. B **31**, 02B103 (2013).

[26] R. D. Young, Theoretical total-energy distribution of field-emitted electrons, Phys. Rev. **113**, 110 (1959).

[27] C. Oshima, Monochromatic field electron emission from a Nb superconductor, Ultramicroscopy **78**, 27 (1999).

[28] K. Yuasa, P. Facchi, R. Fazio, H. Nakazato, I. Ohba, S. Pascazio, and S. Tasaki, Entanglement of electrons field-emitted from a superconductor, Phys. Rev. B **79**, 180503 (2009).

[29] J. B. Xu, K. Läuger, R. Möller, K. Dransfeld, and I. H. Wilson, Energy-exchange processes by tunneling electrons, Appl. Phys. A **59**, 155 (1994).

[30] H. Bergeret, A. Septier, and M. Drechsler, Nottingham effect of a superconducting metal, Phys. Rev. B **31**, 149 (1985).

[31] W. B. Nottingham, Remarks on energy losses attending thermionic emission of electrons from metals, Phys. Rev. **59**, 906 (1941).

[32] R. Gomer and J. K. Hulm, Field emission from tantalum in the normal and superconducting state, J. Chem. Phys. **20**, 1500 (1952).

[33] R. Klein and L. B. Leder, Field emission from niobium in the normal and superconducting states, Phys. Rev. **124**, 1050 (1961).

[34] S. I. Shkuratov, S. A. Barengolts, and E. A. Litvinov, Heating and failure of niobium tip cathodes due to a high-density pulsed field electron emission current, J. Vac. Sci. Technol., B: Microelectron. Nanometer Struct.—Process., Meas., Phenom. **13**, 1960 (1995).

[35] K. Nagaoka, T. Yamashita, M. Yamada, H. Fujii, R. Seo, K. Matsuda, S. Uchiyama, and C. Oshima, Field emission energy spectra from superconducting and normal states of a niobium tip, Ultramicroscopy **79**, 51 (1999).

[36] K. Nagaoka, T. Yamashita, S. Uchiyama, M. Yamada, H. Fujii, and C. Oshima, Monochromatic electron emission from the macroscopic quantum state of a superconductor, Nature **396**, 557 (1998).

[37] J.-L. Hou, W.-T. Chang, C.-C. Shih, Y.-F. Yu, T.-Y. Fu, and I.-S. Hwang, A nanoemitter based on a superconducting material, Appl. Phys. Lett. **108**, 263107 (2016).

[38] K. Nagaoka, H. Ogawa, N. Arai, S. Uchiyama, T. Yamashita, C. Oshima, and S. Otani, Energy distribution of field emission electrons from a niobium ⟨111⟩ tip, Surf. Sci. **357–358**, 218 (1996).

[39] A. D. Pandey, G. Müller, D. Reschke, and X. Singer, Field emission from crystalline niobium, Phys. Rev. Spec. Top.—Accel. Beams **12**, 023501 (2009).

[40] N. Takeuchi and S. Inaba, Refinement of Ta and Nb under UHV conditions, Solid Stat. Phys. **15**, 113 (1980).

[41] D. Biswas, R. Ramachandran, and G. Singh, The tunneling potential for field emission from nanotips, Phys. Plasmas **25**, 013113 (2018).

[42] E. L. Murphy and R. H. Good, Thermionic emission, field emission, and the transition region, Phys. Rev. **102**, 1464 (1956).

[43] J. W. Gadzuk, Resonance-tunneling spectroscopy of atoms adsorbed on metal surfaces: Theory, Phys. Rev. B **1**, 2110 (1970).

[44] M. E. Lin, R. P. Andres, and R. Reifenberger, Observation of the Discrete Electron Energy States of an Individual Nanometer-Size Supported Gold Cluster, Phys. Rev. Lett. **67**, 477 (1991).

[45] V. T. Binh and N. García, On the electron and metallic ion emission from nanotips fabricated by field-surface-melting technique: Experiments on W and Au tips, Ultramicroscopy **42–44**, 80 (1992).

[46] R. Diehl, M. Choueib, S. Choubak, R. Martel, S. Perisanu, A. Ayari, P. Vincent, S. T. Purcell, and P. Poncharal, Narrow energy distributions of electrons emitted from clean graphene edges, Phys. Rev. B **102**, 035416 (2020).

[47] M. Duchet, S. Perisanu, S. T. Purcell, E. Constant, V. Loriot, H. Yanagisawa, M. F. Kling, F. Lepine, and A. Ayari, Femtosecond laser induced resonant tunneling in an individual quantum dot attached to a nanotip, ACS Photonics **8**, 505 (2021).

[48] M. E. Lin, R. Reifenberger, and R. P. Andres, Field-emission spectrum of a nanometer-size supported gold cluster: Theory and experiment, Phys. Rev. B **46**, 15490 (1992).

[49] J. G. Rodrigo, V. Crespo, and S. Vieira, Josephson current at atomic scale: Tunneling and nanocontacts using a STM, Physica C **437–438**, 270 (2006).

[50] L. Hofstetter, S. Csonka, J. Nygård, and C. Schönenberger, Cooper pair splitter realized in a two-quantum-dot Y-junction, Nature **461**, 960 (2009).

[51] Y. Chen, M. M. Doria, and F. M. Peeters, Vortices in a mesoscopic cone: A superconducting tip in the presence of an applied field, Phys. Rev. B **77**, 054511 (2008).

[52] P. G. Kwiat, K. Mattle, H. Weinfurter, A. Zeilinger, A. V. Sergienko, and Y. Shih, New High-Intensity Source of Polarization-Entangled Photon Pairs, Phys. Rev. Lett. **75**, 4337 (1995).

[53] Z. Y. Ou and L. Mandel, Violation of Bell's Inequality and Classical Probability in a Two-Photon Correlation Experiment, Phys. Rev. Lett. **61**, 50 (1988).

[54] T. Jennewein, C. Simon, G. Weihs, H. Weinfurter, and A. Zeilinger, Quantum Cryptography with Entangled Photons, Phys. Rev. Lett. **84**, 4729 (2000).

[55] D. Bouwmeester, J.-W. Pan, K. Mattle, M. Eibl, H. Weinfurter, and A. Zeilinger, Experimental quantum teleportation, Nature **390**, 575 (1997).

[56] P. Walther, K. J. Resch, T. Rudolph, E. Schenck, H. Weinfurter, V. Vedral, M. Aspelmeyer, and A. Zeilinger, Experimental one-way quantum computing, Nature **434**, 169 (2005).

[57] O. Jagutzki, V. Mergel, K. Ullmann-Pfleger, L. Spielberger, U. Spillmann, R. Dörner, and H. Schmidt-Böcking, A broad-application microchannel-plate detector system for advanced particle or photon detection tasks: Large area imaging, precise multi-hit timing information and high detection rate, Nucl. Instrum. Methods Phys. Res., Sect. A **477**, 244 (2002).

[58] J. W. Gadzuk, Many-body tunneling-theory approach to field emission of electrons from solids, Surf. Sci. **15**, 466 (1969).

[59] V. T. Binh and S. T. Purcell, Field emission from nanotips, Appl. Surf. Sci. **111**, 157 (1997).

[60] Y. Saito, S. Kawata, H. Nakane, and H. Adachi, Emission characteristics of niobium nitride field emitters, Appl. Surf. Sci. **146**, 177 (1999).

[61] C. Mechel, Y. Kurman, A. Karnieli, N. Rivera, A. Arie, and I. Kaminer, Quantum correlations in electron microscopy, Optica **8**, 70 (2021).

[62] S. Meier, J. Heimerl, and P. Hommelhoff, Few-electron correlations after ultrafast photoemission from nanometric needle tips, Preprint ArXiv:2209.11806 (2022).

[63] R. Haindl, A. Feist, T. Domröse, M. Möller, S. V. Yalunin, and C. Ropers, Coulomb-correlated few-electron states in a transmission electron microscope beam, Preprint ArXiv:2209.12300 (2022).

[64] I. M. Pop, I. Protopopov, F. Lecocq, Z. Peng, B. Pannetier, O. Buisson, and W. Guichard, Measurement of the effect of quantum phase slips in a Josephson junction chain, Nat. Phys. **6**, 589 (2010).

[65] T. Juffmann, S. A. Koppell, B. B. Klopfer, C. Ophus, R. M. Glaeser, and M. A. Kasevich, Multi-pass transmission electron microscopy, Sci. Rep. **7**, 1 (2017).

[66] W. P. Putnam and M. F. Yanik, Noninvasive electron microscopy with interaction-free quantum measurements, Phys. Rev. A **80**, 040902 (2009).

[67] P. Kruit, R. G. Hobbs, C.-S. Kim, Y. Yang, V. R. Manfrinato, J. Hammer, S. Thomas, P. Weber, B. Klopfer, C. Kohstall, T. Juffmann, M. A. Kasevich, P. Hommelhoff, and K. K. Berggren, Designs for a quantum electron microscope, Ultramicroscopy **164**, 31 (2016).

[68] O. L. Krivanek, J. P. Ursin, N. J. Bacon, G. J. Corbin, N. Dellby, P. Hrncirik, M. F. Murfitt, C. S. Own, and Z. S. Szilagyi, High-energy-resolution monochromator for aberration-corrected scanning transmission electron microscopy/electron energy-loss spectroscopy, Philos. Trans. R. Soc., A **367**, 3683 (2009).